Fast and accurate laser bandwidth modeling of optical proximity effects

Ivan Lalovic*, Oleg Kritsun[1], Joeseph Bendik[2], Mark Smith[3], Chris Sallee[3], Nigel Farrar

Cymer, Inc., 17075 Thornmint Court, San Diego, CA 92127
[1] Advanced Micro Devices, Sunnyvale, CA
[2] Dynamic Intelligence Inc. (DI [2]), Rancho Bernardo, CA
[3] KLA-Tencor, FINLE, Austin, TX

ABSTRACT

In this work, we model the effects of excimer laser bandwidth on optical proximity effects in high-NA ArF dry and immersion lithography. We quantify the errors introduced by using common approximation methods for the laser spectrum, such as the modified Lorentzian and Gaussian forms. Although these approximations are simple to use, and their symmetry properties can lead to reduced simulation run-times, they typically induce significant CD error when compared to the use of measured spectral profiles, which are obtained from high-resolution spectrophotometry. In this paper we establish some accuracy benchmarks and demonstrate the need for inclusion of information about the spectral profile—for the laser type of interest—in order to achieve sub-nanometer image calculation accuracy required for optical proximity correction. We further assess the speed-accuracy tradeoffs in terms of data truncation and sampling, and propose some practical limits for sampling the illumination spectrum.

Additionally, in this work, we propose a new physically-based spectrum approximation method, which significantly reduces computation time at a cost of less than 0.25nm residual image-CD error from the fully-sampled image calculation. In addition to aerial image, we compare 45nm-node calibrated resist models and latent image results for 0.92NA dry and 1.2NA immersion processes using measured illumination profiles and lens aberrations. Finally, we consider the laser bandwidth sensitivity of 2D line-end patterns and typical post-OPC designs for a logic gate-process.

Keywords: excimer, laser, bandwidth, optical, lithography, focus, resolution, chromatic, aberrations, proximity, illumination, Gaussian, modeified Lorentzian

1. INTRODUCTION

The development of water-based immersion lithography equipment (with numerical apertures, NA>1) has enabled continued density scaling of semiconductor devices by providing improved imaging resolution and lower overlay tolerances. The challenges in scaling transistor performance at each technology node have continued to drive the reduction of all process variability sources. Additionally, the performance of CMOS transistors at current technology nodes is leading to an increase in the local transistor-level variability – particularly for microprocessor (MPU) circuits – and will require an even more aggressive improvement in the inherent stability and control of the patterning equipment and materials. Double patterning techniques, which enable scaling for the 32nm node, will require an enhanced level of CD control. Double-patterning overlay (and image placement) errors directly reduce the available CD tolerances and therefore improvements in CD control directly enable higher manufacturing margins, improved device performance and enhanced yields.

The critical lithographic processes, which drive device performance variability, need to be controlled over the lifetime of the manufacturing cycle and therefore lithography imaging stability needs to be maintained over multiple years of production. At the same time, current device tolerances dictate a very

Photomask Technology 2007, edited by Robert J. Naber, Hiroichi Kawahira
Proc. of SPIE Vol. 6730, 67301X, (2007) · 0277-786X/07/$18 · doi: 10.1117/12.746594

high level of process and equipment control. For example, for the 45nm node, the International Technology Roadmap for Semiconductors (ITRS) [1], roadmap cites a total MPU gate-CD control requirement of 1.9nm (3σ). This requirement is inclusive of all sources of patterning CD variability, including mask CD uniformity, optical proximity correction (OPC) accuracy, as well as exposure tool and resist contribution at all spatial length scales (e.g., intra-field, cross-wafer, wafer-to-wafer and lot-to-lot). At the 32nm node, the ITRS total gate-CD control budget is 1.3nm. Given the large number of error contributors, these CD control budgets allow for significantly sub-nanometer errors for the individual error components. In order to maintain target imaging over the process lifetime, at ever decreasing tolerances, lithographers have added focus to areas requiring improved control such as 3D mask topography, measured (polarized) illumination profiles, lens birefringence, as well as bandwidth of the laser illumination source. The variation in these parameters not only affects the CD control directly, but it also diminishes the effectiveness of the optical proximity correction, which must also remain accurate over the lifetime of the process.

1.1 Laser Bandwidth Stability and Metrology

The variability of the excimer-laser bandwidth can substantially affect the variation of critical dimensions—particularly through-pitch imaging—and thus the characterization, metrology and control of bandwidth in the lithography process has been increasing in importance.[2-5] The variation of laser bandwidth modulates the imaging contrast, in turn affecting proximity effects and the validity of OPC models. It has been observed empirically that structures with a more limited depth of focus (DOF) are typically more sensitive to bandwidth variation, but more recently the CD sensitivity to bandwidth has been directly linked to the CD-defocus behavior.[6] Although for typical levels of bandwidth variation the DOF itself is unaffected, it is possible to significantly change the DOF by modifying the shape of the laser spectrum.[7]

A decade of improvement of ArF excimer laser bandwidth stability, shown in Figure 1 below, has supported imaging at the diminishing depth of focus and increasing numerical apertures across generations of lithography systems.

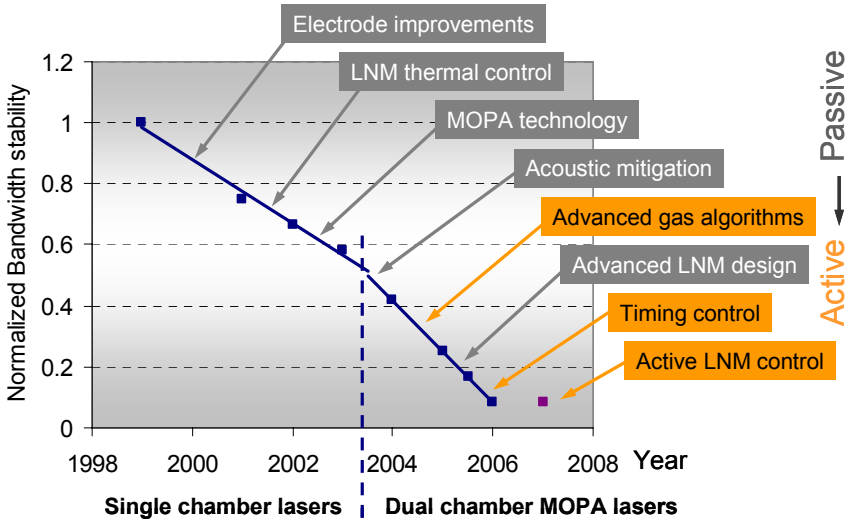

FIGURE 1. Laser bandwidth stability improvement over the last decade

Bandwidth stability has been improved by more than an order of magnitude since first introduction of excimer laser based lithography light sources. Much of the improvement was enabled by development of technologies that inherently reduce the bandwidth variability over lifetime of the components and as a function of operating conditions. This included improved electrode design and materials, improved thermal control of the line narrowing module, chamber designs featuring acoustic mitigation and the master-oscillator power-amplifier (MOPA) system configuration. At the present time, lasers feature closed-loop

control algorithms using multiple actuators, such as gas control, timing and advanced optical adjustments, which enable bandwidth set-point control over a range of operating conditions and lifetime of the laser components.

The increase in numerical aperture for immersion lithography—resulting in DOF of less than 100nm to 200nm—continues to increase the requirements for laser bandwidth stability in both logic and memory processes. Current practical tolerances for OPC error due to bandwidth variation at the 45nm node are less than 1nm,[8] resulting in sub-100fm (1 femtometer = 10^{-15} m) E95 bandwidth variation tolerances. Surpassing this level of bandwidth control can only be realized using active control enabled by high-precision E95 metrology, which is available on-board the latest generation laser systems.[9] The on-board metrology system, together with bandwidth set-point control, allows matching between imaging systems and optimizing OPC throughout the fleet of manufacturing tools. The E95 measurement in the on-board system shows excellent correlation to the in-house spectroscopic techniques over the full range of operating conditions. The high-accuracy spectrophotmetry data is advantageous for accurate lithography modeling where inclusion of the effects of laser bandwidth is desired, and as of recently can be directly programmed in commercial simulation tools (discussed further in Section 2) such as PROLITH™.[10] Due to the complexity of the metrology and sensitivity of the instruments, spectrophotometry of the laser sources is typically only available in the factory. Generalized spectra that typify a class of systems are only now beginning to be introduced for improved OPC modeling.[11]

1.2 Lithography Simulation Accuracy Requirements and OPC

As the industry continues beyond 65nm node manufacturing, lithography simulation enters the domain where the image-model residual errors need to be significantly lower than 1nm (ITRS 45nm node CD accuracy requirement including optical proximity effects is 0.5nm)[1] increasing the importance of understanding computation errors and particularly the quality of the simulation input parameters. Physically-accurate inputs are needed for the optical properties of the imaging medium and photomask topography in addition to characteristic fingerprints of the imaging system. Although, for OPC, calibrated reaction-diffusion resist models are replaced with empirical transfer functions, the imaging model requires equivalent (<<1nm) accuracy so that post-OPC edge-placement errors are minimized. In particular in OPC software, the empirical resist calibration is powerful enough to compensate for inaccuracies of the imaging model. Even in these cases, small cumulative edge placement errors (EPE) following model calibration are achievable, however typically at the expense of OPC robustness – an increase of the OPC sensitivity to variability of the process or imaging setup. Therefore, recent OPC software improvements have been made by integrating inputs of real illumination profiles and projection optics that are representative of a fleet of systems of the same type.

2. THEORY AND SIMULATION METHODS

PROLITH currently enables direct input of measured laser illumination spectra and features a benchmark full brute-force calculation—allowing input of up to 2024 spectrum data points—and several levels of high-speed approximation for imaging using finite laser bandwidth. This capability allows the user to determine the optimum sampling strategy and directly determine the speed-accuracy tradeoffs for the given application.

2.1. Modeling Laser Spectral Bandwidth

The effect of finite laser bandwidth is typically modeled as an incoherent superposition of weighted aerial images over a range of defocus values. The defocus values depend on the longitudinal chromatic aberration (LCA), sometimes termed chromatic defocus, which determines the amount of defocus for a given change in wavelength. The image weights at each wavelength value are given by the laser spectrum. Mathematically, we want to evaluate the following integral in order to obtain the final image intensity $I(x,y,z; f_0)$ at a nominal focus f_0 over the laser spectral distribution $S(\lambda)$ and for a given

LCA, described by the slope of the defocus-wavelength relationship, $LCA = \Delta f / \Delta\lambda$, and where *x, y,* and *z* are the Cartesian spatial coordinates:

$$I(x,y,z;f_0,S(\lambda)) = \int_{-\infty}^{\infty} I(x,y,z;f_0 - LCA\cdot\lambda)\cdot S(\lambda)\cdot d\lambda \quad \text{(equation 1).}$$

We can express the wafer-plane focus distribution *P(f)*, or focus blur, due to the laser spectrum *S(λ)*, by performing the following transformation $S(\lambda_i) \rightarrow P(f_i) = P\left(f_i = \lambda_i \cdot LCA = \lambda_i \cdot \frac{\Delta f}{\Delta\lambda}\right)$.

Therefore, the wafer-plane focus distribution, *P(f)*, is a function of the laser spectrum and the longitudinal chromatic aberration of the projection optics. The LCA value is a constant (over the typical wavelength tuning range of lithography exposure systems) and is determined by the lens material dispersion, refractive power and optical path length, therefore varying for different optical lens designs (or different scanner models). Consequently the same laser spectral output on two different scanner models will scale the width of the wafer-plane focus distribution, *P(f)*, by the ratio of the respective projection optics LCA values. Alternatively, two different laser spectral shapes, *S(λ)*, will lead to proportionally different focus distributions on scanners of the same model. The bandwidth of the laser spectrum, whether it be full-width-at-half-maximum (FWHM) or 95-percent-energy-integral (E95%), can be scaled to obtain the width of the wafer-plane focus distribution by,

$$FWHM_{P(f)} = \frac{\Delta f}{\Delta\lambda}\cdot FWHM_{S(\lambda)}, \text{ or } E95\%_{P(f)} = \frac{\Delta f}{\Delta\lambda}\cdot E95\%_{S(\lambda)}.$$

For example, given an LCA of 300nm/pm, a laser bandwidth FWHM of 0.12pm and E95 of 0.26 results in a wafer-plane focus blur FWHM of 36nm and E95 width of 78nm. From our experience, and reported elsewhere in literature,[3,5] the typical range of LCA, values for modern lithography scanners is 200nm/pm to 500nm/pm.

The concept of a focus distribution (focus blur), or focus probability density function, *P(f)*, is useful because in addition to longitudinal chromatic aberration and laser bandwidth, additional distributions of focal positions can arise from sources such as stage tilt (in the direction of the scan), stage vibrations in the z-direction, in addition to in-scan z-position motion of the wafer stage for focus compensation. Mathematically, all of these effects can be added to a cumulative focus distribution *P(f)* by either straight addition (for the systematic sources such as laser bandwidth, stage tilt and z-scan) or addition in quadrature (for the random errors such as vibrations) of the individual distributions. Furthermore, the cumulative focus distribution formalism allows a straightforward way to include any or all of these effects with a single image calculation. We can thus re-write equation 1, more generally:

$$I(x,y,z;f_0,P(\hat{f})) = \int_{-\infty}^{\infty} I(x,y,z;f_0 - \hat{f})P(\hat{f})d\hat{f} \qquad \text{(equation 2).}$$

When evaluating equation 2 above, one can simply approximate the integral with a standard computational algorithm, such as the rectangle rule or Simpson's rule[12], where the interval is broken into discrete steps in focus δf. In this case, the integral is then computed by a direct summation over the discrete steps in focus. In PROLITH, this approach is available when the main Speed Factor (SF) is set to -1, and the rectangle rule summation step δf is coincident with the available data in the laser illumination spectrum file. This "brute force" approach is useful for detailed calculations where the raw data is evaluated directly. When the main SF is set above -1 (SF>-1), or if no laser spectra are used, a more sophisticated quadrature integration algorithm is used to significantly accelerate the calculation. The accuracy of the final image is dependent on both the main SF approximation setting and complexity of the input illumination spectrum form. The run-time and aerial image accuracy tradeoffs between the different main SF settings have been considered previously.[13] In this paper, we additionally examine the resist simulation run-time and accuracy implications for SF -1, 0 and 1, when approximated spectra are used (in Section 3).

2.2. Modified Lorentzian and Gaussian Laser Spectrum Approximations

In addition to using actual measured laser spectra, the modified Lorentzian (or Cauchy) approximation of the laser spectrum has been used for the purposes of lithography simulation.[5,14] The modified Lorentzian form is typically expressed as

$$ML(\Delta\lambda) = \frac{(FWHM_{ML})^n}{|2\cdot\Delta\lambda|^n + (FWHM_{ML})^n}.$$

Here, n and $FWHM_{ML}$ are the free fitting parameters to the measured spectrum and $\Delta\lambda$ is the wavelength offset from nominal or peak intensity. The $FWHM_{ML}$ parameter corresponds to the full-width-at-half-maximum of the modified Lorentzian.

Although it may seem intuitive to match the *FWHM* of the modified Lorentzian to the *FWHM* of the measured laser spectrum and separately fit the exponent n, better lithographic fits of the laser spectrum are done by simultaneously fitting *FWHM* and n to match the desired width of the energy integral, for example the width of the 95% energy integral. Additionally, minimizing the intensity differences between the modified Lorentzian and the measured data can provide additional refinements to find optimum modified Lorentzian parameters.

The Gaussian form (normal probability distribution), or a more complex combination of Gaussian and modified Lorentzian, have also been suggested[15] as refinements of the above that may improve the fitting of modern laser spectra. However, even the best fits to the data using the modified Lorentzian or Gaussian fail to describe the behavior of real laser spectra particularly in the region of the tails, as seen in Figure 2. Figure 2-a shows the best modified Lorentzian and Gaussian fits to a measured XLA 300 spectrum with an E95 of 0.24pm; the plot in Figure 2-b is the same data plotted on a logarithmic scale.

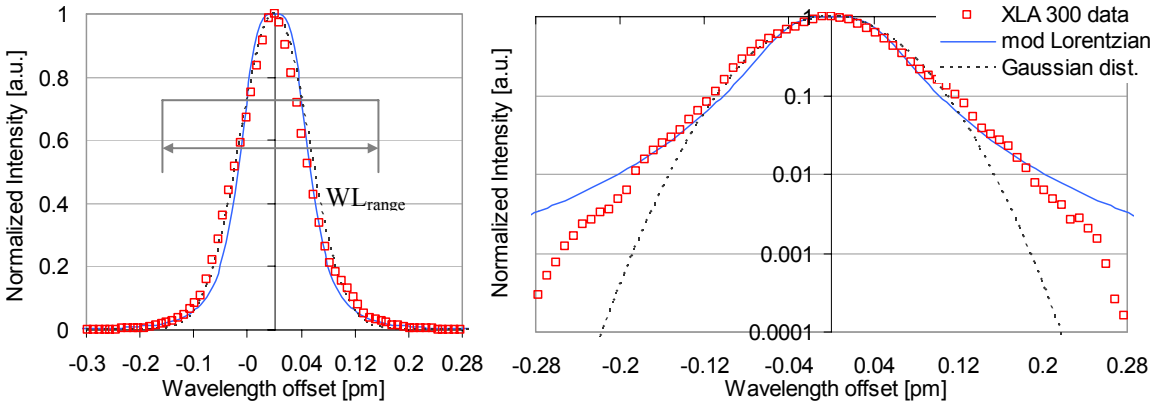

Figure 2- a **Figure 2- b**

FIGURE 2. XLA 300 laser spectra together with best fit modified Lorentzian and Gaussian

Here, the E95 fitting is performed over a 5pm wavelength range to ensure accurate energy integration well away from the main spectral feature. In this case the best-fit Gaussian distribution fits the sample XLA 300 spectrum better than the modified Lorentzian, particularly for normalized intensities greater than approximately 2%. Neither the modified Lorentzian nor Gaussian approximation is particularly accurate in describing the spectrum tails (beyond 0.75xE95 or less than 1% of normalized intensity). In the following section, we explore the lithographic implications of using the analytic forms and we quantify the minimum integration range, WL_{range}, (depicted in Figure 2-a) that is required to achieve a desired level of simulation accuracy.

3. RESULTS

3.1. Laser Spectrum Sampling Requirements

To determine the sampling requirements for laser spectra, simulations are performed as a function of wavelength (WL) range for a number of measured spectra. The different spectra have varied E95 widths and cover a wide range of spectral shapes. The image integration (equation 1) terminates when the WL range parameter is exceeded (shown in Figure 2-a). Figure 3 shows the simulated lumped parameter model (LPM) CD as a function of the spectrum truncation range for an isolated feature imaged at 1.2NA with c-quadrupole illumination and 6% attPSM 100nm mask structure (in the Kirchhoff or thin-mask approximation). The isolated CD is clearly more sensitive to certain laser spectra shapes and in those cases requires a larger WL integration range to obtain the same level of CD accuracy—'spectrum A', for example, does not converge to within 0.1nm until a WL range of 1.5pm. In Figure 4, we plot the first derivative of the CD data (in Figure 3) with respect to the WL range.

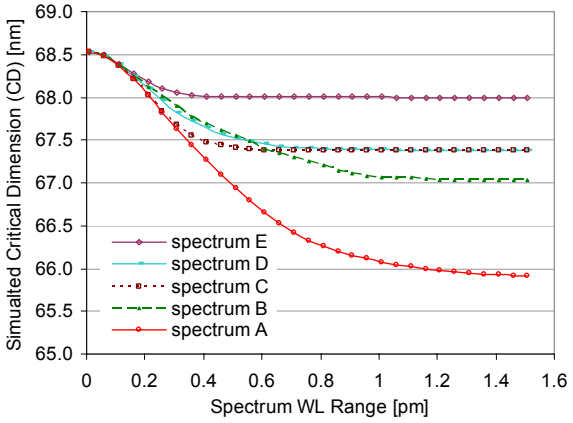

FIGURE 3. CD as a function of simulation WL_{range}

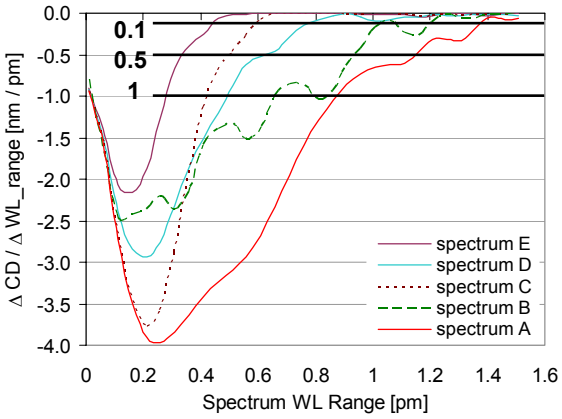

FIGURE 4. Change of CD vs. WL_{range}

The slope of the CD change as the integration range is useful, since it allows quantifying the width of the spectrum that is needed to achieve a desired CD convergence level, as depicted by the 0.1nm, 0.5nm and 1nm levels. We can therefore read out the spectrum WL range level required to get a specific level of CD convergence per 1pm change in the WL range. For the five spectra, A through E, the WL range required is plotted in Figure 5 as a function of E95 bandwidth for the corresponding spectra.

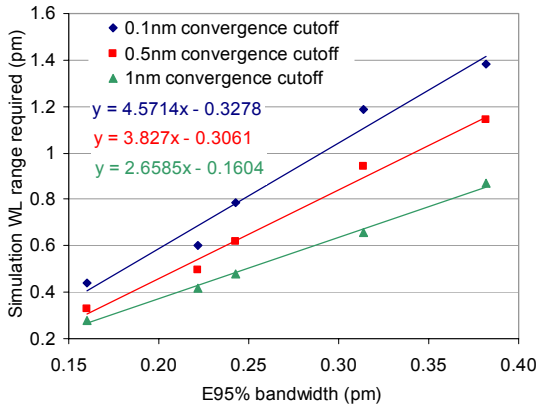

FIGURE 5. E95 scaling of error-convergence criteria

As shown in this figure, we see that the simulation WL range needed to achieve the desired convergence level scales linearly as a function of E95 bandwidth of the spectrum used for that particular simulation. Therefore, in general, for simulations using spectra with larger bandwidth values, an increased WL integration range is needed to achieve the same CD accuracy. The slope of the line, for each convergence

criteria, can be used to determine the integration range needed. For example, in order to maintain the CD convergence below 0.1nm (per 1pm of WL range), the WL integration range needs to extend to 4.6 x E95% (pm) of the laser spectrum used in the simulation. For CD accuracy of 0.5nm (per 1pm of WL range), which may rarely be the integration range required is 3.8 x E95% (pm). For typical E95% values of current MOPA systems, where the E95% bandwidth is lower than 0.5pm, this means that the spectrum data should include a wavelength range greater than ~2pm for simulations with sub 0.1nm simulation accuracy. This result points to the sensitivity of the lithographic result on the low intensity tails of the spectrum, particularly if high accuracy image simulation is required. Unfortunately, as the WL range of the simulation is increased, the simulation time increases as well. For the 'brute force' calculation method, described in Section 2 (implemented in PROLITH as main SF = -1), the simulation time grows linearly with the integration interval. In the following sections we therefore propose alternate methods for reducing simulation time while maintaining accuracy at the sub-nanometer level.

Although here we have shown the result for isolated lines in the lumped parameter resist model, the accuracy scaling with E95 bandwidth holds for aerial image threshold simulation as well and dense features with no loss of generality— for dense features the absolute CD sensitivity to bandwidth is typically lower. The scaling between simulation accuracy and integration range is not significantly sensitive to the shape of the spectrum even for atypical spectral profiles; the accuracy scaling is mainly dependent on the E95 bandwidth.

3.2. Imaging Differences between Real Laser Spectra and Modified Lorentzian fits

The modified Lorentzian form has been popular among some lithographers for representing the imaging effects of the laser spectrum, because it often results in faster simulation time (due to symmetry properties). Given assumptions about the value of the exponent, this form can be used to simply scale the bandwidth to different E95 values by scaling the FWHM parameter. However, as discussed in Section 2, this is not a very good predictor of real laser spectra, particularly in the tail region of the spectra—the region to which the imaging results are most sensitive—and is no better description of the spectrum shape than a simpler Gaussian form with a single fitting term.

The differences in imaging are apparent when comparing the through-pitch and through-focus CD differences between simulations done using a real laser spectrum input and the best-fit to the spectrum data using the Modified Lorentzian form, as shown in Figure 6-a and 6-b.

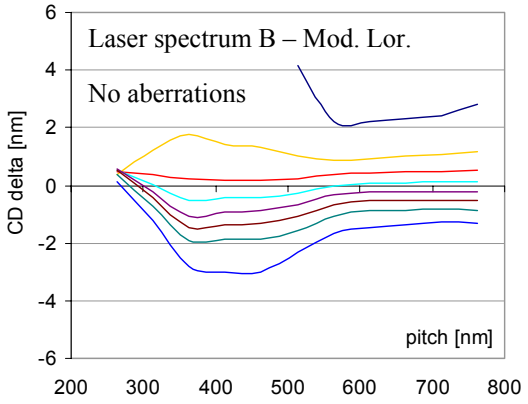

FIGURE 6- a. ML - raw spectrum CD differences No aberration

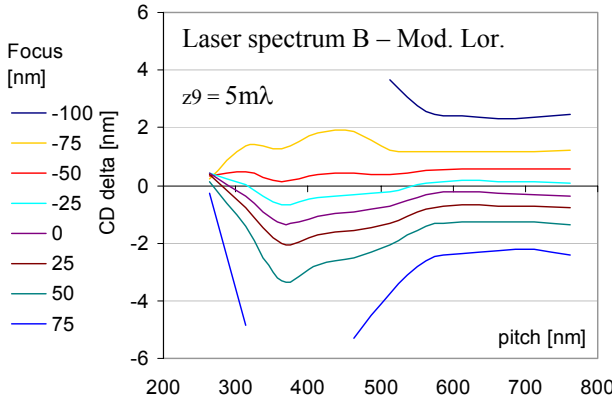

FIGURE 6- b. ML - raw spectrum CD diff. 5mλ spherical aberration (Z9)

The aerial image threshold CD differences between the modified Lorentzian best-fit (FWHM= 0.26 and n= 2.8) and an actual laser spectrum (consisting in this case of 1000-pts) for the XLA 105 laser model are as large as 5nm (Figure 6- a) over a 150nm range of focus settings. When projection lens aberrations are added (Figure 6- b), in this case 5-miliwave primary spherical (Z9 Zernike), the same input spectra

comparison yields CD errors greater than 8nm~10nm. These images are computed for dry lithography with a numerical aperture of 0.92 and 0.6/0.8 30-degree c-quad illumination targeting 65nm binary structures. For 45nm structures, using water immersion at 1.2NA with same c-quad illumination mode as above, the image-threshold CD differences through-pitch and through-focus between a full (measured) XLA 300 spectrum and a Gaussian best-fit input spectrum are shown in Figure 7- a. The CD errors for a Modified Lorentzian best-fit input (compared to the same measured XLA 300 spectrum) are shown in Figure 7- b.

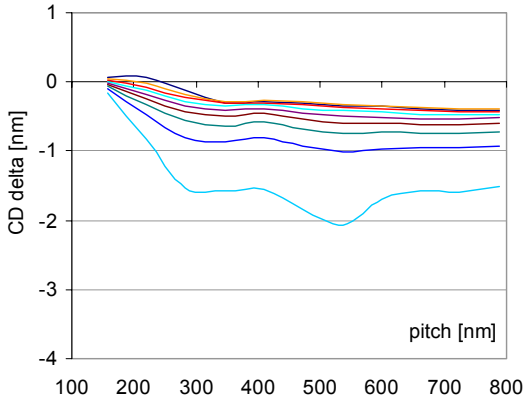

FIGURE 7- a. CD delta, XLA300- Gaussian

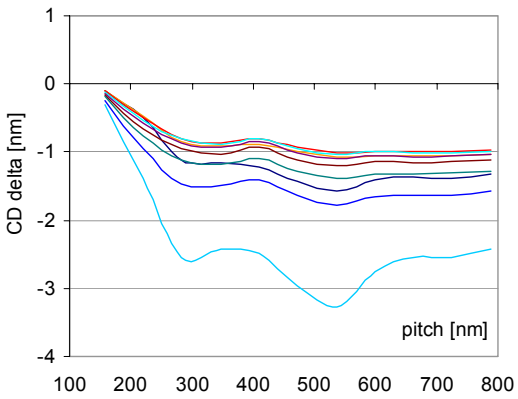

FIGURE 7- b. CD delta, XLA300- Mod. Lorentzian

The Gaussian fit to this spectrum data set results in lower CD errors than a modified Lorentzian for the same imaging condition. In addition to the iso-dense bias errors of ~1.5nm and ~2.5nm, for the Gaussian and modified Lorentzian respectively, both fitting methods fail to capture the more subtle (0.5nm~1nm) through-pitch structure that results form the real laser spectra.

3.3. Lithographically Accurate Laser Spectrum Approximation (LSA)

So far, we have seen that reducing the laser spectrum integration range (Section 3.1) or using analytic fitting functions (Section 3.2) results in CD errors exceeding several nanometers for both aerial images and lumped parameter resist model. In order to include a diffusion-reaction resist model, or for 2D mask layout, it is highly desirable to reduce run-times for simulation of laser bandwidth effects, while maintaining sub-nanometer accuracy. We have therefore investigated several methods to minimize the speed-accuracy tradeoff. In this section, we describe an empirically-based method for approximating the measured spectrum data, which often contain thousands of data points. The result of this approach is a 25-point laser spectrum approximation (LSA), shown in Figure 8, for an XLA 300 spectra at three levels of E95 bandwidth.

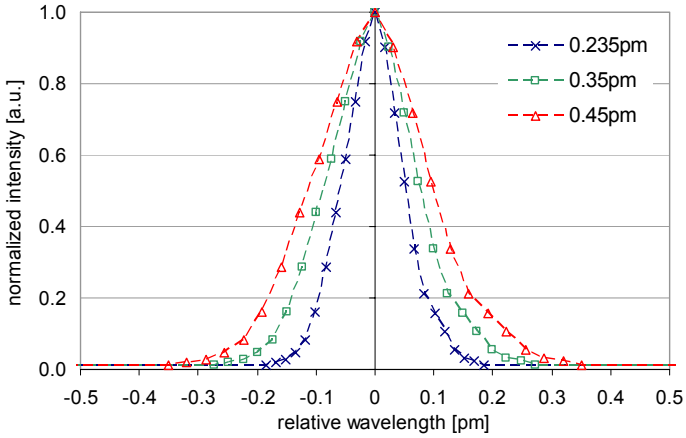

FIGURE 8. Laser Spectrum Approximation (LSA) using 25pts

In practice, the bandwidth scaling can be accomplished optically using the tunable active bandwidth stabilization (ABS) for either running a fleet of lasers at a fixed E95 or as variable set-points in an OPC-matching strategy. Prior to the development of ABS, other experimental techniques have been employed to measure the lithographic imaging results.

The LSA is obtained by iteratively re-sampling of the full (measured) laser spectrum, reducing the number of data points (typically starting with thousands, limited only by the physical sampling of the spectrophotometer) to the target 25-points that lithographically best describe the response of the full spectrum through pitch and through focus. Because of the re-sampling, the very important contribution of the laser spectrum tails is approximated by an artificially elevated level of a flare-like DC image offset. This 'computational' DC image intensity is also determined iteratively as a part of the re-sampling algorithm and, for the spectra we have approximated to date, typically ranges between 0.2% and 0.8% of the energy of the total spectrum. (Note: this is much larger than the typical measured spectrum background, which is $<10^{-4}$ energy). In PROLITH, this can be simulated by a second-pass open-frame exposure or by introducing an appropriately scaled flare intensity level. Another approach is add to the wavelength integral two additional aerial images, which are significantly defocused (>750nm from best focus) to have an essentially flare-like contribution. The aerial image CD differences between the LSA and the full measured spectrum to which the LSA is fitted—in this case the approximation is iteratively performed to fit an XLA 105 spectrum—are shown in Figure 9-a and 9-b.

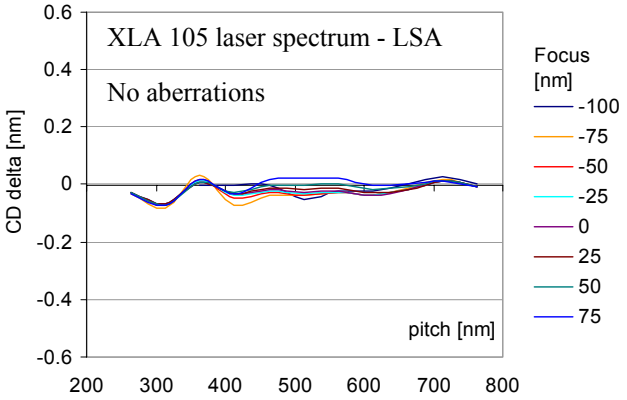

FIGURE 9- a. Full spectrum - LSA CD differences No aberration

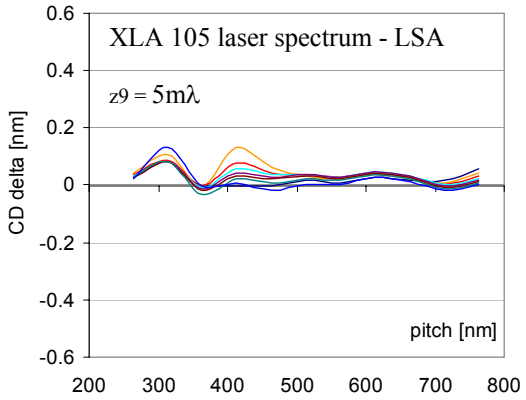

FIGURE 9- b. Full spectrum - LSACD diff 50mλ spherical aberration (Z9)

The CD residuals, following the approximation, are significantly sub-nanometer. Even when 5mλ spherical aberration is added, the residual error is virtually unaffected for the same LSA and same measured spectrum data. These CD errors should be contrasted with the results of the best-fit modified Lorentzian in Figure 6. Additionally, for a number of different spectra, the robustness of the match between the LSA and the measured data is verified over differing illumination conditions and dry/immersion NA's in Figure 10-a and 10-b.

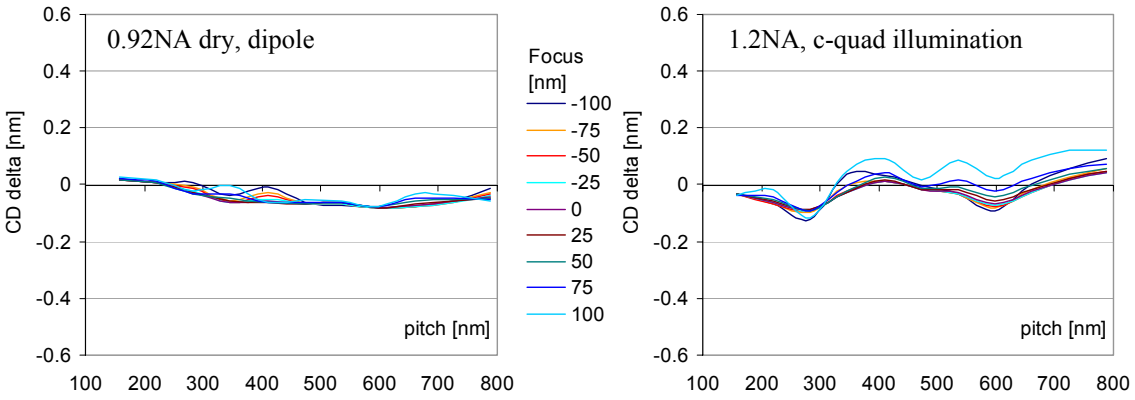

FIGURE 10- a. Measured spectrum - LSA

FIGURE 10- b. Measured spectrum - LSA

In Figure 10, continuing with the same LSA and measured spectrum data, the comparison is done for different illumination and lens NA conditions. The CD residuals are calculated for a 0.92NA and dipole illumination (0.6 center sigma / 0.2 pole radius sigma) and 1.2NA immersion c-quad illumination (the latter is possible only in the world of simulation, given that this particular laser combination is unlikely). In these cases, the aerial image CD differences between the spectrum approximation and the full physical spectrum input are typically lower than 0.3nm (TIR). At the same time, simulations using the LSA input are between 20 to 100 times faster than full laser bandwidth simulation in PROLITH, with the actual improvement in speed depending on specific model assumptions.

Similar CD error analysis has been extended to 1.35NA immersion, a range of illumination conditions, attenuated-PSM and binary mask structures. In all of these cases the through-focus and through-pitch CD differences remain at the levels cited above indicating that the robustness of the fit is sufficient and allowing application of the same approximated spectrum to a range of imaging situations. We have additionally studied the CD differences as a function of a linearly scaling the LSA and corresponding full spectra—for example, studying bandwidth adjustment using Tunable-ABS (active bandwidth stabilization) for the XLA 300 laser model—showing no significant CD differences over a range of spectral shapes. Although not shown here, we are confident that scaling the LSA input can be used to model the effects of laser bandwidth changes (for a fixed spectral shape) without loss of accuracy from the computationally expensive full-spectrum simulations. As we will discuss further in the following section, resist effects can often lead to differences compared to aerial (or aqueous) image threshold CD's, and although the optimum LSA is normally determined based on iterations that minimize the image threshold-CD errors, the LSA is just as valid for photoresist CDs.

3.4. Imaging Effects in Photoresist Due to Laser Bandwidth

The improvement in simulation speed using the spectrum approximation approach, described in the previous section, enables the study of laser bandwidth effects for 2D mask patterns and full diffusion-reaction (calibrated) photoresist models in practical run times. The following figure, Figure 11, shows that, in addition to aerial and lumped-parameter model results, the LSA approach maintains sub-0.2nm accuracy for photoresist images.

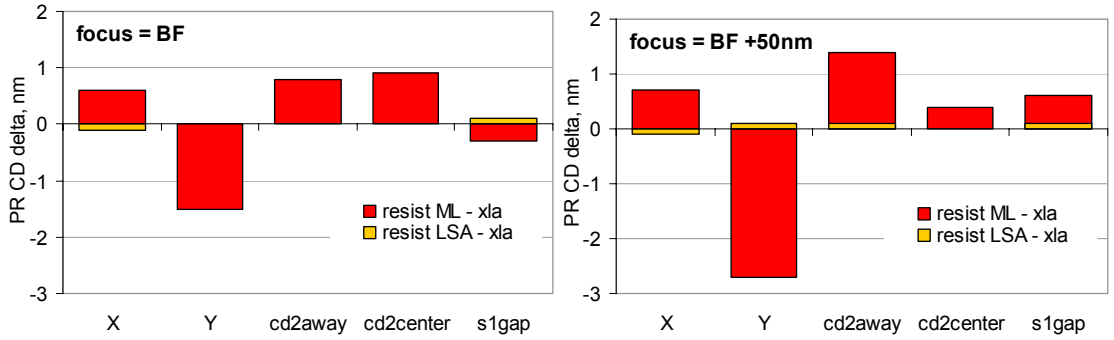

FIGURE 11. Photoresist (PR) model CD differences between the real XLA spectrum and a) modified Lorentzian (ML) as well as b) laser spectrum approximation (LSA) for best focus (BF) and 50nm defocus

In Figure 11, we plot photoresist (PR) model CD errors for structures (cut-lines from a 2D clip) for the 45nm design rule for the 2D binary mask layout shown in Figure 12, which is repeated due to the periodic boundary condition of the simulation domain. The imaging setup consists of a 1.2NA immersion objective, annular illumination (0.9 / 0.99 σ_{in} / σ_{out}) and PAR IM850 calibrated resist model in PROLITH (the main speed factor set to 0 or -1, and the longitudinal chromatic aberration is set to a value corresponding to existing 1.2NA_{max} scanners). Even for the PR CD results, the LSA accuracy compared to the full laser spectrum is extremely good. Compared with the modified Lorentzian (ML) input, the LSA accuracy is, for some structures, orders of magnitude better and increasingly so for defocused images. The run-time of the LSA resist simulation is 20 to 50 times faster than the using full spectra, therefore it becomes practical to look in detail at bandwidth sensitivity of real 2D post-OPC gate-layout patterns using full reaction-diffusion PR models.

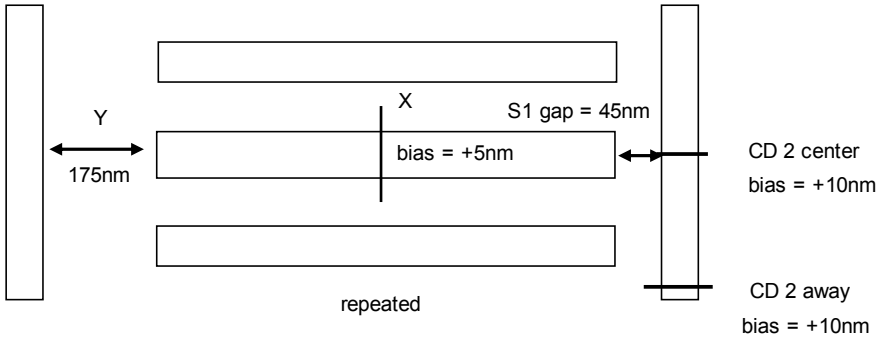

FIGURE 12. 45nm design clip of a 2D layout (cut-lines = X, Y, s1 gap, cd2center, cd2away)

The photoresist model and image-threshold CD sensitivities to the E95 laser bandwidth for four cut-lines (X, Y, CD2center, s1gap) at best focus using the LSA input assumption are shown in Figure 13. The imaging setup is the same as described above.

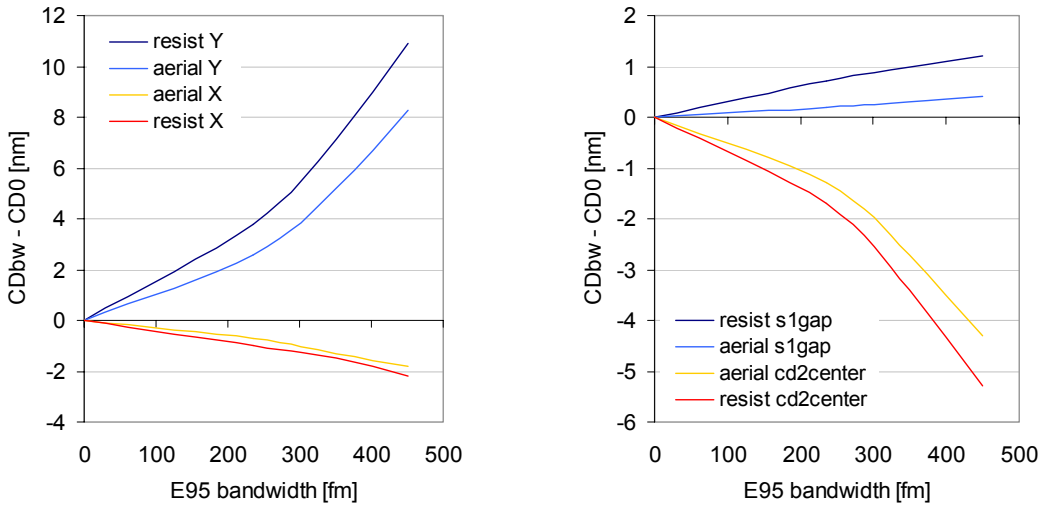

FIGURE 13. Bandwidth - CD sensitivity for 2D patterns (defined in Fig. 12) for PR and aerial

Here we see the typical parabolic behavior of all of the cut-line structures as a function of increasing bandwidth. The sensitivity of the PR structures is generally higher than for aerial (aqueous) images, with the isolated and the ~iso line-ends showing higher sensitivity than dense structures. The total run-time for all 2D bandwidth sensitivity simulations in Figure 13 is 55min using the LSA with main SF setting of 0 (on a 2GHz dual-core x86 mobile processor with 2Gb RAM), while the full-spectrum PR simulations of this 2D domain-size would take 12hours ~ 14hours at the same main SF setting. As a comparison a single monochromatic PR simulation run of this domain takes 10minutes.

4. DISCUSSION AND CONCLUSIONS

In this work we studied the speed - accuracy tradeoff between several assumptions for the input of laser spectrum (or bandwidth) information in PROLITH. The scaling of the normalized (reaction-diffusion) resist simulation speed and the typical (average) through-pitch and through-focus (TFTP) max CD error as a function of laser bandwidth input has been summarized in Figure 14 for 45nm and 65nm logic node simulations of the type presented in this work. For the monochromatic case the max TFTP CD errors are as large as 5nm (sometimes greater for images at the edge of the process window)—the more typical CD errors are on the order of 3nm.

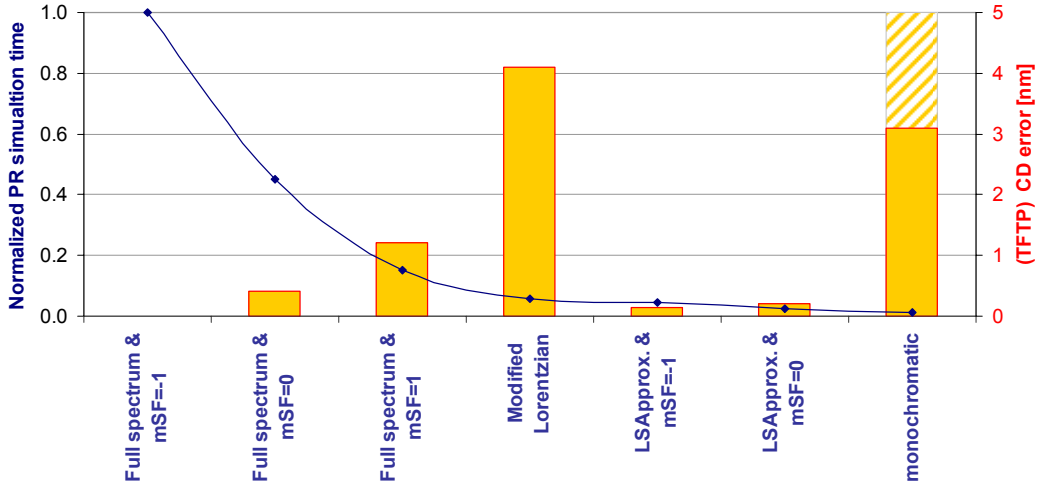

FIGURE 14. Speed - accuracy tradeoff using different laser bandwidth input assumptions

We chose a 1000-point measured spectrum with main speed factor (mSF) setting of -1 to be the accuracy benchmark—from which the TFTP CD errors for aerial and PR images are computed in our studies—and to which the PR simulation run-times are also normalized (Figure 14). The efficient computation approaches reflected in the increasing mSF settings can indeed lead to considerable (2x~6x) improvements in run-time using full-spectrum data, however the CD residuals quickly exceed the sub-0.5nm ITRS simulation requirements for the 45nm node for mSF > 0. On the other hand, the LSA approaches, described in Section 3.3, result in sub-0.25 (TIR) errors for aerial and resist CD images. The run-time improvements of 50x (using mSF=0) are typical, and in some cases up to 100x improvement has been achieved. The commonly-used modified Lorentzian approximation can be useful to investigate general CD trends as a function of bandwidth changes, however the CD errors and therefore the magnitude of the TFTP CD-bandwiwdth sensitivities can be significantly under or over-estimated particularly in the presence of projection lens aberrations. We have shown that the Gaussian approximation can be at least as accurate as the modified Lorentzian and neither considerably advances the accuracy beyond the monochromatic assumption.

The accuracy and run-time improvement of the LSA approach makes viable the study of bandwidth sensitivities for real 2D post-OPC layout clips using physical resist models. The combination of the LSA and mSF=0 results in <15minute PR image runs in PROLITH for domain sizes of up to 1μm, given standard mobile computing platforms. Hardware acceleration and improved computation efficiency can significantly reduce the run-times and other approaches for approximating the laser spectrum input (exploiting non-linear optimization, sample symmetry or TCC convergence) can be considered. Extensions of these LSA approaches in the area of integration with software tools for OPC model generation and process-variability verification are currently being investigated.

ACKNOWLEDGMENTS

The authors graciously thank Robert Rafac and Fedor Trintchouk from Cymer for invaluable discussions of laser spectrometry techniques and data, as well as William Howard from KLA-Tencor and Peter De Bisschop from IMEC for discussion of modeling of laser bandwidth effects. The contribution of Harry Levinson (AMD) and Tommy Oga (Cymer) is recognized for valued review and input to this manuscript.

The authors also express their thanks to KLA-Tencor for the opportunity to work with and provide input on pre-release versions of PROLITH leading to development of raw spectral data input (as of version 9.3.3) and new focus blur features.

REFERENCES

1. *International Technology Roadmap for Semiconductors (ITRS)*, 2006 Update, *Lithography* and *Modeling and Simulation*, http://www.itrs.net/reports.html
2. A. Kroyan et al., "Modeling the effects of excimer laser bandwidths on lithographic performance," Proc. SPIE Optical Microlithography XIV **4000** (2000).
3. I. Lalovic et al., "Effects of illumination spectral width on mask error enhancement factor and iso-dense bias in 0.6NA KrF imaging," Proc. SPIE Phot. Tech. Symp. BACUS XXI **4562** (2001).
4. K. Huggins et al., "Effects of laser bandwidth on OPE in a modern lithography tool," Proc. SPIE Optical Microlithography XIX **6154** (2006).
5. Brunner et al, "Laser bandwidth and other sources of focus blur in lithography," Proc. SPIE Optical Microlithography XIX **6154** (2006).
6. P. De Bisschop et al, to be published.
7. I. Lalovic et al., "RELAX: Resolution Enhancement by Laser-spectrum Adjusted Exposure," Proc. SPIE Optical Microlithogrpahy XVIII **5754** (2005).
8. Yoshimochi et al, "Study of iso-dense bias (IDB) sensitivity to laser spectral shape at the 45-nm node," Proc. SPIE Optical Microlithography XX **6520** (2007).

9. R. Rafac et al, “Overcoming Limitations of Etalon Spectrometers Used for Spectral Metrology of DUV Excimer Light Sources,” Prox. SPIE Optical Microlithography XVII **5377** (2004).
10. PROLITH is a registered trademark of KLA-Tencor, San Jose, CA.
11. G. Bailey et al, “Modeling Laser Bandwidth for OPC Applications“, *to be presented at SPIE Optical Microlithography, San Jose, CA, February 25th - 29th, 2008.*
12. Press, Teukolsky, Vettering, and Flannery, Numerical Recipes in C, 2nd edition, Cambridge University Press (1992).
13. M. Smith et al., "Modeling and performance metrics for longitudinal chromatic aberrations, focus-drilling, and Z-noise: exploring excimer laser pulse spectra," Proc. SPIE Optical Microlithography XX **6520** (2007).
14. Lai et al., “Understanding chromatic aberration impacts on lithographic imaging,” *Journal of Microlithography, Microfabrication, and Microsystems,* **2**-2, *pp105-111* (2003).
15. R. Rafac, private communication